An integrate-and-fire model to generate spike trains with long memory

Alexandre Richard, Patricio Orio, Etienne Tanré

An integrate-and-fire model to generate spike trains with long memory

Alexandre Richard * Patricio Orio † Etienne Tanré ‡

May 12, 2017

Abstract

Long-range dependence (LRD) has been observed in a variety of phenomena in nature, and for several years also in the spiking activity of neurons. Often, this is interpreted as originating from a non-Markovian system. Here we show that a purely Markovian integrate-and-fire (IF) model, with a noisy slow adaptation term, can generate data that appears as having LRD with a Hurst exponent (H) greater than 0.5. A proper analysis shows that the asymptotic value of H is 0.5 if a long enough sequence of events is taken into account. For comparison, we also consider a new model of individual IF neuron with fractional noise. The correlations of its spike trains are studied and proved to have long memory, unlike classical IF models. On the other hand, to correctly measure long-range dependence, it is usually necessary to know if the data are stationary. Thus, a methodology to evaluate stationarity of the interspike intervals (ISIs) is presented and applied to the various IF models. In conclusion, the spike trains of our fractional model have the long-range dependence property, while those from classical Markovian models do not. However, Markovian IF models may seem to have it because of apparent non-stationarities.

Key words: Interspike-interval statistics, Stochastic Integrate-and-Fire model, Long-range dependence, Stationarity.

1 Introduction

The modelling of neuronal activity has a long and rich history whose first successes date back to the 50's and the seminal work of [23]. A few years later, a simpler probabilistic model based on the passage times of a random walk was introduced by Gerstein and Mandelbrot [21], corresponding to a stochastic version of the Perfect Integrate-and-Fire (PIF) model. It is noticeable that the second author is also at the origin of the theory of fractals and long-range dependence, but never applied these concepts to neuroscience.

The activity of a neuron is characterised by the electrical potential of its membrane, and more precisely by spikes whose amplitude and duration are very similar to one another. Therefore, it

*CMAP, Ecole Polytechnique, Route de Saclay, 91128 Palaiseau, France; alexandre.richard@polytechnique.edu. Research supported by the ERC 321111 Rofirm. Part of this work was carried out while A.R. was a postdoc at Inria Sophia-Antipolis.

†Instituto de Neurociencia, Facultad de Ciencias, Universidad de Valparaíso and Centro Interdisciplinario de Neurociencia de Valparaíso, Universidad de Valparaíso, Chile; patricio.orio@uv.cl.

‡Université Côte d'Azur, Inria, 2004 Route des lucioles BP 93, 06902 Sophia-Antipolis, France; Etienne.Tanre@inria.fr.

A.R. and E.T. acknowledge the support from the ECOS-Sud Program Chili-France C15E05 and from the European Union's Horizon 2020 Framework Programme for Research and Innovation under Grant Agreement No. 720270 (Human Brain Project SGA1). P.O acknowledges the support from the Advanced Center for Electrical and Electronic Engineering (Basal Funding FB0008, Conicyt) and the project P09-022-F from the Millennium Scientific Initiative of the Chilean Ministry of Economy, Development, and Tourism.

is rather the sequence of times at which these spikes occur which is believed to carry the neuronal information. While temporal (and spatial) correlations between interspike intervals (ISIs) have been observed for a long time (see Chacron et al. [10] and references therein), the presence of fractal behaviour (Teich [54], Bair et al. [2]) and *long-memory* phenomena in the spiking activity of neurons has been acknowledged for only two decades: see Teich et al. [55], Teich et al. [56], Lewis et al. [26], Lowen et al. [29], including artificially grown neuronal networks in Segev et al. [49], etc. (see the introduction of Jackson [24] for a very comprehensive list of references). This long memory phenomenon is ubiquitous in nature, and takes the form of power-law correlations between interspike intervals rather than exponentially decaying correlations. In particular, long memory implies that the present neuronal activity is correlated with a very distant past.

Until recently in the neuroscience literature, long memory, also called long-range dependence (LRD), has been quantified mostly by the Fano factor. In [4], temporal and spatial LRD of *in vivo* human hippocampal neurons is detected relying on statistics like the detrended fluctuation analysis [37]. We shall adopt a similar approach, which has also been used to detect LRD in ion channels [13]. LRD may be due to the influence of presynaptic neurons, as well as intrinsic factors such as fluctuations in ion channel activity (producing long-range dependence in neurotransmitter exocytosis, as described by Lowen et al. [28]). Schwalger et al. [48] also mention several possible sources of LRD: neural refractoriness, bursting and adaptation.

Early attempts to replicate the LRD property of ISIs were based on point processes models and were proposed by Teich [54], Bair et al. [2], and more recently Jackson [24]. Instead, we focus here on stochastic Integrate-and-Fire models, especially because they allow to preserve the aforementioned interpretation on the origin of LRD. Besides, it is commonly accepted that they provide a good compromise between biologically complex and realistic models such as the Hodgkin-Huxley model, and more simple and amenable ones to perform statistical computations with.

Brunel and Sergi [6] and Destexhe et al. [16] noticed that an additional differential equation for the synaptic current, coupled with the membrane potential equation of a simple IF model, introduces temporal correlations in the dynamics. Assuming that the pre-synaptic excitation is modelled by a Poisson noise, it is natural by diffusion approximation to write the synaptic equation as a stochastic differential equation driven by white noise. An interesting feature of this model is that it is simple enough to compute (or approximate) some ISI statistics: for example, Middleton et al. [35] focused on the ISI density, power spectral density and Fano factor of the PIF, Lindner [27] on serial correlation coefficients of the PIF, Schwalger and Schimansky-Geier [46] on the ISI density, coefficient of variation, Fano factor of the leaky integrate-and-fire (LIF) model, etc. We also refer to Sacerdote and Giraudo [44] for a mathematical and statistical treatment of Markovian IF models.

The purpose of this paper is to explain that an IF model with Markovian noise, even enhanced with a synaptic variable, has exponentially decaying correlations which cannot produce long-range dependent ISIs. To account for different correlation patterns observed on real data, we introduce an IF model governed by fractional Brownian noise. The fractional Brownian motion (fBm) is a stochastic process whose increments (the noise process) are long-range dependent and stationary. It naturally appears in modelling as a limit of more simple processes: For instance, the fBm appears as the limit of high-dimensional Orstein-Uhlenbeck processes [9], see also [3, 32, 33, 34, 52] for other constructions. However, it is non-Markovian, which makes it a challenge to study and compute all the aforementioned statistics of spike trains. A similar point of view is developed in Schwalger et al. [48], where general Gaussian processes are proxied by finite-dimensional Markov processes and serve as input in an IF model. We also discuss the approach of Sobie et al. [50] which is based on $1/f$ noise.

In addition to modelling, our contribution is also methodological: we compare several measures of LRD and stationarity. Indeed, testing stationarity is important in the attempt to measure LRD, as we shall see that non-stationary spike trains from Markovian models can give

the illusion of LRD. We refer to Samorodnitsky [45] and Beran et al. [3] on these questions, as well as the collection of review articles edited by Rangarajan and Ding [41] on modelling long-range dependent phenomena in various fields ranging from economy, biology, neuroscience to internet traffic. Last but not least, one is often interested in getting estimates on the distribution of the ISIs. But without the stationarity assumption, these distributions are likely to vary with time, which makes the estimation procedure either difficult or inaccurate. Hence, it is crucial to determine if these distributions vary with time, as it is desirable that the sequence of ISIs be in a stationary regime for such study. We therefore explain how to test this assumption, with a direct application to ISIs generated by integrate-and-fire models.

The remainder of the paper is organized as follows: in Section 2, we present an account of the tools and methods to measure LRD and stationarity from a single spike train. Then the stochastic Integrate-and-Fire models and some of its variations are presented in Section 3, with an emphasis on fractional noise. The results or our analysis are detailed in Section 4.1 for the Markovian PIF with adaptation, in Section 4.2 for the PIF with fractional noise, and in Section 4.3 for variants with mixed Brownian and fractional noise. Finally, we discuss these results and compare them to previous models in Section 5.

2 Methods: Statistical measurement of long-range dependence and stationarity

2.1 Long-range dependence

The terminology "long memory" or "long-range dependence" appeared in the early work of Mandelbrot and coauthors in the 60's (Mandelbrot [33], Mandelbrot and Wallis [32], etc.), in an attempt to describe the phenomenon observed by Hurst on the flows of the Nile river.

If X is a random variable or a stochastic process, we say that $X(\omega)$ is a realization (or an observation) of X for the outcome ω in the probability space Ω of all possible outcomes. Let us denote by $\mathbb{E}$ the expectation of a random variable. A sequence of random variables $\{X_n\}_{n\in\mathbb{N}}$ has the *long-range dependence (LRD)* property if it satisfies:

$$\sum_{n=1}^{\infty} \mathbb{E}\left[(X_1 - \mathbb{E}X_1)(X_n - \mathbb{E}X_n)\right] = +\infty.$$

Observe that the LRD property is obtained by averaging over all possible outcomes. In practical situations though, where we might have access to very few realizations (or even a single one) of the same phenomenon, at least two limitations appear: the length of the sequence is finite, and we do not know the law of the X_n's (in fact when dealing with spike trains, we often have one sample of the sequence). To detect long-range dependence, we will use two estimators: the detrended fluctuation analysis (DFA) and the rescaled range statistics (R/S). There exist other popular methods to measure the Hurst parameter (properly defined in Section 2.1.1), but as seen from [53, 57] we may not expect to get much better results than with the DFA and R/S methods. Besides, the latter is the only statistics for which it has been possible to prove convergence to the Hurst parameter rigorously in some non-trivial cases as the number of observations goes to infinity [3, 45].
To prove convergence of the R/S statistics, it is usually required that the sequence $\{X_n\}_{n\in\mathbb{N}}$ is L^2-stationary, in the sense that

$$\text{for all } n, \quad \mathbb{E}(X_n) = \mathbb{E}(X_1) \qquad \text{and} \qquad \text{for all } n \geq m, \quad \mathbb{E}(X_n X_m) = \mathbb{E}(X_{n-m+1} X_1), \tag{1}$$

although there are examples of such convergence for non-stationary data ([5] and [45, p.183–185]). Verifying this requirement is often eluded in practical situations, although non-stationarity

may have important consequences on the interpretation of statistical analysis of data. We will see that indeed in our numerical experiments, our model can produce non-stationary spike trains. Nevertheless, the R/S and DFA statistics seem to converge even without this condition. We emphasize that measuring (non-)stationarity and long-range dependence is usually a tricky question.

Let us insist on the type of data we shall be dealing with: these are (finite) sequences $X_1, \dots, X_N$ (we now use this notation both for the probabilistic model and a realization of it). We aim at obtaining the Hurst parameter of the data from a single sequence (i.e. not from averaging several realizations), to cope with biological constraints.

2.1.1 The rescaled ranged statistics (R/S)

For a sequence $\{X_n\}_{n\in\mathbb{N}}$ of random variables, let $\{Y_j = \sum_{i=1}^{j} X_i\}_{j\in\mathbb{N}}$ denote the sequence of the cumulated sums, and let the rescaled-range statistics be defined as:

$$R/S(N) = \frac{\max_{1\le i\le N}(Y_i - \frac{i}{N}Y_N) - \min_{1\le i\le N}(Y_i - \frac{i}{N}Y_N)}{\sqrt{\frac{1}{N}\sum_{i=1}^{N}(X_i - \frac{1}{N}Y_N)^2}} \ .$$

If for some $H \in (0,1)$, $\frac{1}{N^H}R/S(N)$ converges towards some positive random variable denoted by $e^{\mathbf{b}}$, we call H the Hurst parameter of the model. In the most simple example, where the X_n's are independent and identically distributed (*iid*) with finite variance, the convergence occurs with $H = \frac{1}{2}$. We consider that data have long-term memory when $H > \frac{1}{2}$ (the reverse case $H < \frac{1}{2}$ is often called anti-persistence, but we will not encounter it here).

Let us recall that N denotes the length of the sequence of data $X_1, \dots, X_N$. A simple way to estimate H is to fit the following linear model for various values of N:

$$\log R/S(N) = \mathbf{b} + H \ \log N \ .$$

However this is not the robust way to proceed in practice (see [3, 53, 57]). Instead, we divide the data into M blocks of length n ($N = M \times n$) and compute the R/S statistics on each block $\widetilde{R/S}(m,n)$ for $m = 1 \dots M$. Then, we average over all blocks to obtain $\widetilde{R/S}(n) = \frac{1}{M}\sum_{m=1}^{M}\widetilde{R/S}(m,n)$. Finally we let n take integer values between 1 and N and estimate the slope of the function $n \mapsto \widetilde{R/S}(n)$. This slope gives the estimated Hurst parameter of $\{X_i\}_{i\le N}$, frequently denoted by $\hat{H}_N$ in the rest of this paper.

Let us conclude this paragraph with several insightful examples:

- If the X_n's are iid and $\mathbb{E}\left(X_n^2\right) < \infty$, then standard convergence results imply that $\frac{1}{\sqrt{N}}R/S(N)$ converges to B, where B is an explicit functional of the Brownian bridge.
- If the X_n's are mixing and stationary, then $H = 1/2$ (see Section 5.2).
- If the X_n's are the increments of a fractional Brownian motion with scaling parameter α (*fBm*, see Section 3.1), then α is also the Hurst parameter, i.e. $\frac{1}{N^\alpha}R/S(N)$ converges.

Remark 2.1. *There are examples of sequences of random variables with infinite variance such that $\frac{1}{\sqrt{N}}R/S(N)$ converges ([45, p.178–180]). There are also examples of non-stationary random sequences for which the R/S statistics converges at prescribed rate $H \in [\frac{1}{2}, 1)$, see Samorodnitsky [45, p.187].*

2.1.2 The detrended fluctuation analysis (DFA)

This method was introduced by Peng et al. [37, 39] in genetics. We merely rephrase [57] to present it. See also [53] where it is called Residuals of Regression method and where it is compared to other methods.

Like in the R/S analysis, the data are divided into M blocks of length n. For $m = 1 \dots M$ and $j = 1 \dots n$, we denote the partial sum on block m by $Y_{m,j} = \sum_{i=1}^{j} X_{(m-1)n+i}$. On each block, a linear regression is applied to determine coefficients (a_m, b_m) such that $\tilde{Y}_{m,j} := a_m j + b_m, j = 1 \dots n$ is the least-square approximation of $Y_{m,j}$. Then, the empirical standard deviation of the error is computed:

$$s_m := \sqrt{\frac{1}{n} \sum_{j=1}^{n} \left(Y_{m,j} - \tilde{Y}_{m,j} \right)^2}.$$

Finally, the mean of these standard deviations is $\bar{s}_n := \frac{1}{M} \sum_{m=1}^{M} s_m$. The analysis performed with $\widetilde{R/S}(n)$ can now be reproduced with $\bar{s}_n$ (ie the heuristics is that $\bar{s}_n$ behaves asymptotically as a constant times n^H). The slope computed from the log-log plot is again denoted by $\hat{H}_N$.

2.1.3 Surrogate data

To check for the statistical significance of the R/S and DFA analyses, we employed a bootstrapping with replacement procedure. For each simulated spike train, we produced 100 sequences of spikes by randomly shuffling the interspike intervals of the spike train. In this way, we obtain 100 new spike trains having the same interspike interval distribution, but without any correlation structure between spikes. The LRD analysis is applied to these new data to estimate $\hat{H}_N$ as a function of N for each of them. The mean over each surrogate sample is plotted (see Figure 1D) in a black solid line, while two gray lines represent the mean $\pm$ 2 times the standard deviation. Thus, the region between gray lines will contain roughly 95% of possible H values that can be obtained by chance from a non-correlated data series. If the plot of $\hat{H}_N$ of the initial spike train enters this shadow region, then it is doubtful that the data has the LRD property.

2.2 Stationarity

It is in general a difficult problem to decide whether data are issued from a stationary distribution or not. Like the measurement of long-range dependence, part of the difficulty here arises from the fact that we want to decide whether biological data are stationary relying on a single observation (i.e. a single sequence of spikes). A frequently used test for stationarity is the KPSS test [25], based on unit root testing. However, we found unit root tests to perform badly when used on fractional noise (which is stationary).

Here we used some other tests for stationarity: a simple windowed Kolmogorov-Smirnov (KS) test, the Priestley-Subbha Rao (PSR) test and a wavelet-based test. Note that notion of stationarity itself must be clarified: the first test (KS) evaluates *strong stationarity*, i.e. whether the law of the process is invariant by any time shift. The PSR and wavelet-based tests consider a weaker form of stationarity that we shall refer to as *L^2-stationarity*. A process X is L^2-stationary if it satisfies (1). It is important to have in mind that the best test to use in a given situation depends strongly on the type of non-stationarity of the data (see for instance Table 2 in [7]). Since we do not know *a priori* what type of non-stationarity may appear, we are applying several tests.

Like for the Hurst estimation of the previous section, these tests are designed to be run on a single realization of the process (said otherwise, no averaging is needed), which is well-suited for biological data. However, to decide whether a model yields stationary spike trains, multiple simulations can be performed. Hence the PSR and wavelet-based tests were repeated 50 times and a boxplot of the p-values was plotted. If the data come from a model which produces stationary ISIs, p-values must be uniformly distributed between 0 and 1. Otherwise we may conclude that the law is not stationary.

Thus, this methodology is designed to decide whether our models produce stationary ISIs. If the problem is to decide whether a single (biological or simulated) sequence is stationary, such stationarity tests will merely give a probability that the sequence is stationary.

2.2.1 The windowed Kolmogorov-Smirnov (KS) test

Based on the usual Kolmogorov-Smirnov (KS) test, we designed a windowed KS test. In this test, the ISI series are split in windows of fixed time length. Each block is tested against the others to see if they are described by the same distribution, using the non-parametric KS test. For each pair, the p-value is then represented in a two-dimensional table. The null hypothesis is that the two samples are drawn from the same distribution. Hence, small p-values indicate that the data may be non-stationary. In this way, a visual map is obtained in which one can easily detect portions of the time series that do not follow the same distribution as the others. Since this test does not return a single p-value, it is not suited to the aforementioned methodology of repeating simulations. Yet it allows for simple interpretations and we keep it for comparison with other tests.

2.2.2 The Priestley-Subbha Rao (PSR) test

Let $X = \{X_t\}_{t\in\mathbb{R}}$ be a centered stochastic process with finite variance. It is known that if X is L^2-stationary, then

$$X_t(\omega) = \int_{\mathbb{R}} e^{ift} A(f)\ Z_\omega(\mathrm{d}f),$$

where $Z = \{Z_\omega(B),\ \omega \in \Omega, B \in \mathcal{B}(\mathbb{R})\}$ is a random measure on $\mathbb{R}$ and A is the spectral density function. A natural generalization of the definition of X_t is to let A depend in time. The PSR test [40] evaluates the time dependence of $A_t(\cdot)$. Thus, a test is proposed with the following null hypothesis: $t \mapsto A_t(f)$ is constant in time.

Assumptions on the data: zero mean (data can be centered in practice), finite variance, "almost" Gaussian. More precisely, if $\mu(\mathrm{d}f)$ denotes the spectral measure associated to Z (i.e. $\mathbb{E}(|Z(B)|^2) = \mu(B)$ for any Borel set B of $\mathbb{R}$), the evolutionary spectral density of X is $D_t(f) := |A_t(f)|^2 \frac{\mathrm{d}\mu(f)}{\mathrm{d}f}$. An approximation of $D_t(f)$ can be computed from the data, and is denoted by $\hat{D}_{t_i}(f_j)$ for discrete values $t_1, \ldots, t_N$ and $f_1, \ldots, f_M$.

A two-factor analysis of variance is performed. First the interaction sum of square is tested: if the p-value is small, then the test can stop here, since the data are non-uniformly modulated, and thus are non-stationary (see [40]). Otherwise, the data are uniformly modulated and one can proceed to test the stationarity. Under each null hypothesis, the test statistics are simple chi-square distributions (with different degrees of freedom).

2.2.3 A wavelet-based test

This test [8] is designed for a large class of processes called locally stationary wavelet processes (LSWP), which can be written:

$$X_t(\omega) = \sum_{j=1}^{\infty} \sum_{k=-\infty}^{\infty} \theta_{j,k}\psi_{j,k}(t)\xi_{j,k}(\omega),$$

where $\{\psi_{j,k}(t), t \in \mathbb{Z}\}$ is a wavelet basis, $\{\xi_{j,k}\}$ is an array of iid random variables with mean 0 and variance 1, and $\{\theta_{j,k}\}$ are the (deterministic) wavelet coefficients of X.

First compute the discrete wavelet coefficients $d_{j,k} = \sum_{t=1}^{T} X_t\psi_{j,k-t}$ and the wavelet periodogram $I_{j,k} = d_{j,k}^2$. The quantity of interest is then the β-spectrum defined by the family of coefficients $\beta_j(\frac{k}{T}) = \mathbb{E}(I_{j,k})$, which form intuitively the evolutionary wavelet spectrum (up to a

linear transform) of the signal. Since we do not have access to the mathematical expectation directly from the data, an approximation of β is proposed in [36].

The process $\{X_t, t = 1, \ldots, T\}$ is stationary if and only if for all j, $\beta_j(z)$ is constant. We refer to Nason [36], Cardinali and Nason [8] and references therein for intermediate results and methodology of the analysis of the $\beta_j(z)$.

The PSR test and this wavelet test give excellent results when applied to pure fractional noise, in the sense that they repeatedly give large p-values, as expected.

2.3 Numerical tools

To test stationarity, we relied upon *Python*'s function `stats.ks_2samp` from the `scipy` library for our windowed KS test, and upon the couple of *R* packages:

- for the PSR test, we have used the *R* package `fractal`, and particularly the function `stationarity`.
- for the wavelet-based test, we have used the function `BootWPTOS` from the *R* package `BootWPTOS`.

The implementation of the methods to measure the Hurst parameter are standard (see Section 2.1), and we used our own *Python* code.

3 The models

We describe a large class of noisy integrate-and-fire models with adaptation. Integrate-and-fire models have two regimes. The *subthreshold regime* is characterized by the stochastic differential system

$$\begin{aligned} \mathrm{d}V_t &= (\mu_V - \lambda_V V_t + \gamma Z_t)\,\mathrm{d}t + \sigma \mathrm{d}B_t^\alpha \\ \mathrm{d}Z_t &= (\mu_{Z,t} - \lambda_Z Z_t)\,\mathrm{d}t + \sigma' \mathrm{d}\tilde{B}_t^\alpha. \end{aligned} \tag{2}$$

The process $(V_t, t \geq 0)$ models the membrane potential and $(Z_t, t \geq 0)$ corresponds to an extrinsic synaptic current with adaptation. We call Z the adaptation variable/process, even though in several cases we remove the adaptation part. μ_V, λ_V, λ_Z, γ, σ, σ' and α are parameters of the model. We detail the role of $\mu_{Z,t}$ in the next paragraph. μ_V is the input current or Voltage offset; λ_V is the relaxation rate of the voltage (the inverse of membrane time constant); γ is the coupling factor between the adaptation variable Z_t and V_t; λ_Z is the relaxation rate of the adaptation (inverse of time constant); σ and σ' are the intensities of the noises B^α and $\tilde{B}^\alpha$ – random noises called fractional Brownian motions and described further in Paragraph 3.1.

$\mu_{Z,t}$ is an offset factor for Z. We will either consider that $\mu_{Z,t}$ is constant in time ($\mu_{Z,t} \equiv \mu_Z$) or that it varies during 1 ms only after a spike ($\mu_{Z,t} \equiv \mu_Z + \epsilon_{Z,t}$). In both cases, let us remark that the law of $(V_t, t \geq 0)$ remains invariant by the modification of parameters $(\mu_Z, \mu_V) \to (\mu_Z + a, \mu_V - \gamma\frac{a}{\lambda_Z})$. So, to reduce the number of parameters to estimate, we assume that $\mu_Z = 0$. In the second case (adaptation), we thus have $\mu_{Z,t} = \epsilon_{Z,t}$, where $\epsilon_{Z,t}$ is positive during 1 ms after a spike and 0 otherwise.

The *firing regime* is activated at the times τ when the membrane potential hits a fixed (deterministic) threshold V^{th}. We call such a time τ a firing time. Just after τ, the membrane potential is *reset* to a fixed value V^{r}, the rest potential. At the same time, we recall that $\mu_{Z,t}$ can be incremented due to adaptation. This puts a natural limit to Z, mimicking the behavior of a finite population of ion channels [47]. The sequence of firing times is formally defined for $n = 1, 2, \ldots$ as

$$\tau_n = \inf\{t \geq \tau_{n-1} : V_t = V^{\mathrm{th}}\}$$

and $\tau_0 = 0$. The sequence of interspike intervals is $\{X_n = \tau_n - \tau_{n-1}\}_{n\in\mathbb{N}}$, consistently with the notations of Section 2.

From a mathematical point of view, the membrane potential is a càdlàg process[1], like the adaptation process Z (which is even continuous), meaning essentially that these processes are right-continuous in time. This is the most commonly used framework to enable the definition of solutions (V_t, Z_t) to Equations (2).

Remark 3.1. *More hidden states like Z can be added in (2) to approximate Gaussian processes which have long-range correlations (see [48] where this idea is fully developed, and Subsection 4.3.3 where we test it numerically).*

3.1 The noise

In Equation (2), the noises $(B_t^\alpha, t \geq 0)$ and $(\tilde{B}_t^\alpha, t \geq 0)$ are fractional Brownian motions (fBm) of scaling parameter $\alpha \in (0, 1)$. By definition, they are Gaussian centered processes with covariance function

$$\mathbb{E}\left[B_t^\alpha B_s^\alpha\right] = \frac{1}{2}\left(|t|^{2\alpha} + |s|^{2\alpha} - |t-s|^{2\alpha}\right).$$

The case $\alpha = 1/2$ corresponds to the standard Brownian motion (integral of white noise). This stochastic process has already been applied in various fields of physics and more recently, biology: in the context of biological dynamics (cell movement in crowded environment, so-called anomalous diffusions), see for instance [34], [11] and [41]. More generally, fractional Brownian motion provides a good, mathematically tractable, model of so-called $1/f$ noise, see e.g. [1]. $1/f$ noise has been successfully applied to describe many phenomena, from heartbeat [38] to internet traffic [58], including neuronal fractal dynamics [29, 50].

Contrary to standard Brownian motion, the fBm with $\alpha \neq \frac{1}{2}$ is not Markovian, which makes the computation of even basic statistics of ISIs a very difficult problem. However when $\alpha > \frac{1}{2}$, the increments of the fBm (i.e. the fractional noise) have positive correlations decaying very slowly, according to a power law:

$$\begin{aligned}\mathbb{E}\left[B_1^\alpha (B_{n+1}^\alpha - B_n^\alpha)\right] &= \frac{1}{2}\left((n+1)^{2\alpha} + (n-1)^{2\alpha} - 2n^{2\alpha}\right)\\ &\sim 2\alpha(2\alpha-1)n^{2\alpha-2}.\end{aligned}$$

This is the long-range dependence property we shall include in our models. The case $\alpha < \frac{1}{2}$ also yields power-law correlations, but negative, which is not useful here.
Very little is known on the first-passage time (equivalent here to spiking time) of models such as (2) driven by fractional Brownian motion: for the passage-time of fBm itself, see [15] for simulations and formal estimation of the density when α is close to $\frac{1}{2}$ and [14] for inequalities on its Laplace transform, and on the general model see [43] for inequalities on Laplace transforms.

3.2 Models without the Z variable ($\gamma = 0$)

When $\gamma = 0$, (2) is a noisy Leaky Integrate-and-Fire (LIF) model. The particular case $\lambda = 0$ corresponds to the noisy Perfect Integrate-and-Fire (PIF) model. The membrane potential is solution of a linear stochastic differential equation. In the white noise setting $\alpha = 1/2$, the interspike intervals are independent and identically distributed, so in particular such sequences are stationary.

[1] continu à droite, limite à gauche, in French, see [42].

Remark 3.2. *1. Compared with multidimensional Markov models (see 4.3.3), this model is also more compact. This can be interesting when one needs to estimate the parameters from real data (see [44]).*

2. We have also chosen to consider a model without any refractory period. The results seem to be interesting even in this simplified case.

3.3 Simulation tools

We simulated the subthreshold regime (2) with a simple Euler scheme implemented in *Python*. The hitting times are then recorded each time the simulated value of V reaches a value above the threshold, according to the firing regime described above.

However, there is no simple and efficient algorithm to simulate fractional Brownian motion. For our simulations, we chose the most efficient *exact* algorithm[2], namely the Davis-Harte algorithm (explained for example in [12]). We used Dieker's `C` code for this algorithm [17].

4 Study of LRD and Stationarity of the simulated data

4.1 PIF model with stochastic adaptation

4.1.1 Long-range dependence

We simulated a spike train using a Perfect Integrate-and-fire (PIF) model, i.e. (2) with $\lambda_V = 0$. The voltage dynamic is deterministic ($\sigma = 0$) and the slow adaptation variable (Z) has an additive noise ($\sigma' = 2.5\text{e}{-6}$). In this case, $\alpha = 0.5$, meaning the noise is standard white noise (no correlation).

Figure 1A shows the spikes and the intervals obtained in a 500 s-long realization of the model, which yielded 15,164 spikes for a firing rate of approximately 30 spikes/sec (and a mean ISI of 33ms with standard deviation of 4.5). The Rescaled Range statistics and Detrended Fluctuation analyses were first applied to a shorter sequence of intervals, the first 100 s (3,023 spikes) of simulation. Figure 1B shows that the common linear regression between $\log n$ and $\log R/S(n)$ or $\log DF(n)$ yields a H value near 0.75 in both cases, suggesting a long-range dependence of the ISI sequence. However, this data was generated with a model that is of Markovian nature.

Visual inspection of the plots reveals that the slope calculated is far from being the asymptotic slope, and that the curve 'bends' toward the right end. When we included the full sequence to the R/S and DFA analyses (Figure 1C), it is evident that the points are not following a linear relationship and the calculated slopes are lower. To characterize better the non-asymptotic nature of the slope, we repeated the fit in sliding windows of 15 points. Three of such fits are shown as continuous lines in Figure 1C (note that in Figure 1C every other point has been omitted) and Figure 1D depicts a plot of the slopes found as a function of the length of the sequence. From this figure, it is clear that for both R/S and DFA the actual asymptotic behavior is a slope of 0.5. As the sequence length n increases, the slope approaches the 0.5 value and, moreover, gets into the 2*standard deviation range calculated from surrogate data (see 2). Thus, only the analysis of a very large sequence of data —probably discarding the shorter sequences in the analysis— will reveal that what appears to be long-range dependence has only a limited time span and that the phenomena underlying it is ultimately Markovian. Nevertheless, even on reasonably large sequences, we see that the Hurst estimator $\hat{H}_n$ is decreasing with n in the Markovian model (Figures 2 and 3), while it is relatively stable in the fractional case, as we shall see later (Figure 6). In the following, the R/S analysis is no longer displayed in the plots. The reason is that we systematically observed a similar quantitative behaviour between the R/S

[2] this algorithm has complexity $O(n \log n)$.

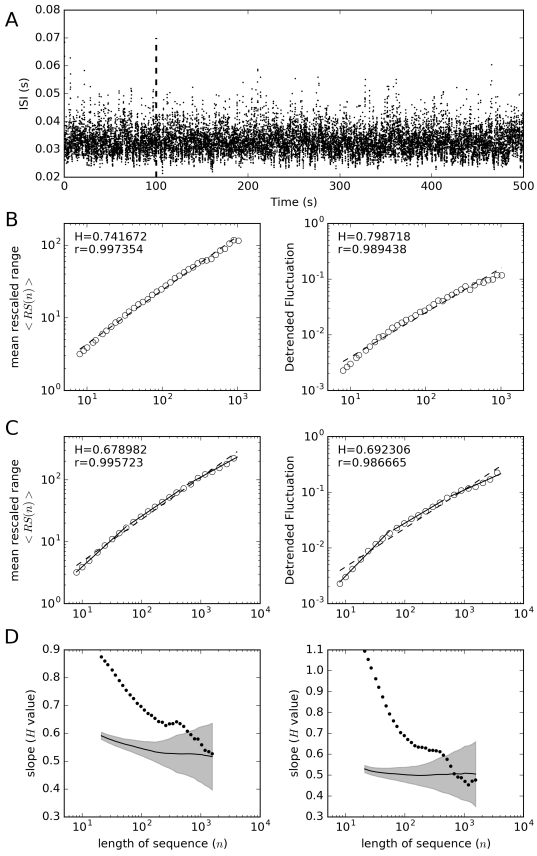

Figure 1: R/S and DFA analysis of PIF model with noisy adaptation. **A** ISI sequence analyzed. parameters are $\mu_V = 0.04$, $\lambda_V = 0$, $\gamma = 0.3$, $\sigma = 0$, $\lambda_Z = 0.005$, $\sigma' = 2.5\text{e}{-6}$. The vertical segmented line shows the limit of the data analyzed in (B). **B** Rescaled range (left) and Detrended Fluctuation Analysis (right) for the ISIs in the first 100 seconds of simulation (3023 spikes). H value is the slope of the best fit of $\log n$ vs. $\log R/S(n)$ or $\log DFA(n)$ points to a straight line (segmented line over the data points). **C** R/S and DFA analysis of the full ISI sequence (15164 spikes). The H values indicated in the top left corner, and the segmented lines correspond to the fit of the full set of points to the data as in (B). The shorter, continuous lines depict the best fit of a subset of the points. **D** Slope values calculated at different n values (with a moving window of 7 points), for the R/S (left) and DFA analysis (right). The continuous line shows the mean slope calculated with 100 surrogate series and the shadow region shows the empirical Standard Deviation of the surrogate data slopes.

and the DFA, hence it was not necessary to keep both. We chose the DFA over the R/S for its better accuracy (see Figure 8).

The apparent long-range dependence of the data is largely related to the stochastic nature of the adaptation. Figure 2A shows that the apparent LRD is lost when the noise is present only in the voltage equation ($\sigma > 0$) but not in the adaptation ($\sigma' = 0$). When the noise is present in both equations, the apparent LRD is somewhat reduced for high values of σ (Figure 2B). Also, Figure 2B shows an interesting case where visually the straight line seems to be a good fit of the $\log n$ versus $\log DFA(n)$ data (and the associated r coefficient seems also good). However, the bottom plot shows how the $H > 0.5$ situation is only transitory for the shorter sequences

and the asymptotic value actually falls within the standard deviation for the shuffled data. On the other hand, the magnitude of the noise seems not to affect much this behavior (Figure 2C and D).

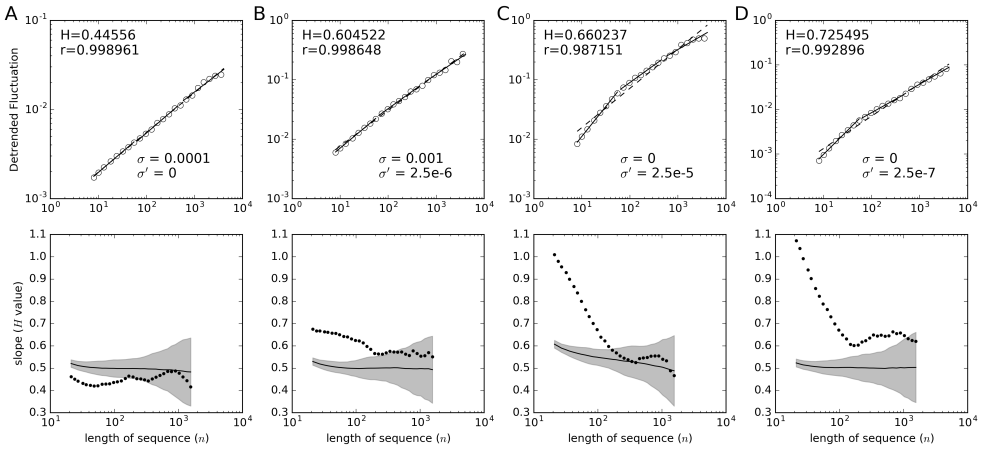

Figure 2: Hurst estimation depending on the different sources of noise. Detrended Fluctuation Analysis of simulations with noise only in the voltage equation (**A**), in both the Voltage and the Adaptation equation (**B**), and in the Adaptation equation (**C** and **D**) with two values of σ'. Panels are as described in Figure 1C and 1D (right).

The LRD is also linked to the rate constant for slow adaptation, λ_Z. Figure 3 shows that a large rate (or a small time constant $\tau_Z = 1/\lambda_Z$) is associated with the loss of apparent LRD (Figure 3A), while a smaller value produces a LRD that is maintained for longer sequence lengths and also a higher H value (Figure 3B). Further parameter explorations revealed that in order to observe the apparent LRD, the time constant for slow adaptation has to be at least twice the mean interval between spikes (not shown).

Figure 3C explores the situation where the adaptation variable Z is no longer updated at each spike (i.e., $\mu_{Z,t} = 0$ for every t). In this case, Z_t can be understood as a correlated noise (in the form of an Ornstein-Uhlenbeck process) added to the variable V. Although the adaptation effect is lost and the firing rate is increased (not shown), the apparent LRD is still present, showing that it is the correlated nature of the stochastic variable that causes this effect. This is very much in line with what has been described for other statistics of firing in the presence of different forms of correlated noise [47, 48].

4.1.2 Stationarity

We base our stationarity analysis of the spike trains on the windowed KS, PSR and wavelet tests. For the PSR and wavelet tests, we apply the methodology described in Section 2, hence in each panel of Figure 4, the left bar is a boxplot of 50 p-values from the PSR test computed from 50 independent spike trains generated by the same model; the right bar does the same with the wavelet test. On the other hand, Figure 5 shows the results of the windowed KS test for a single realization of the models indicated.

In the PIF model with stochastic adaptation, a lower adaptation rate λ_Z (longer adaptation time constant) is associated with a loss of stationarity, i.e. the data windows are no longer described by the same distribution (Figures 4(a)-(c) and 5A). It seems that a lower adaptation rate λ_Z (corresponding to a larger relaxation time $1/\lambda_Z$) produces a sequence of ISIs farther from stationarity, and that $1/\lambda_Z$ not only characterizes the speed of convergence of Z_t to its

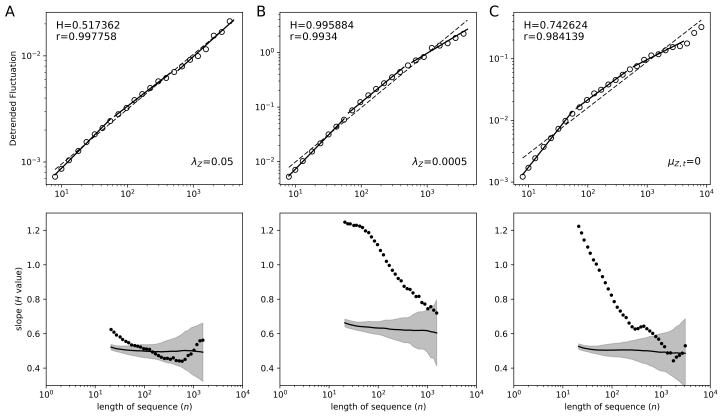

Figure 3: Dependency of the LRD on adaptation parameters. **A.** Effect of a shorter time constant ($\tau_Z = 1/\lambda_Z$). **B.** Effect of a longer time constant. **C.** Long-range dependence analysis in the absence of adaptation, i.e. the Z variable is not affected by the occurrence of spikes.

stationary regime, but also the speed of convergence of the law of the ISIs to theirs.

On the other hand, adding only white noise to the dynamics of V produces stationary data (Figures 4(d) and 5A).

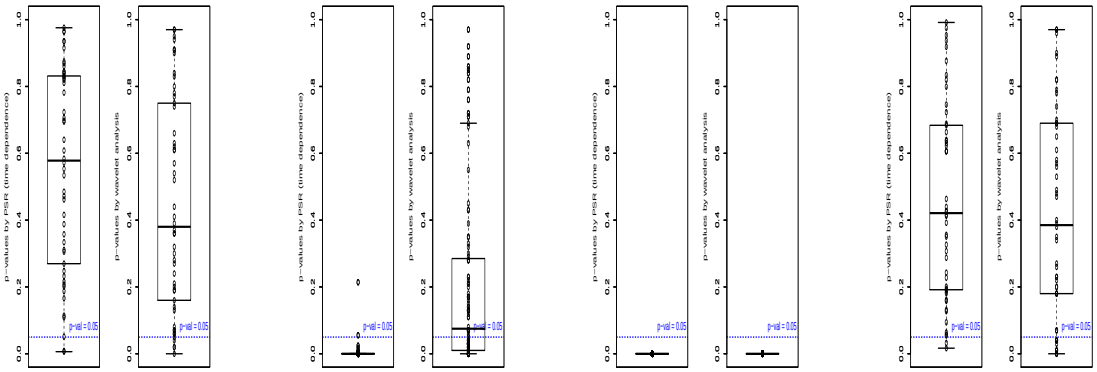

(a) $\lambda_Z = 0.05$ (b) $\lambda_Z = 0.005$ (c) $\lambda_Z = 0.0005$ (d) $\sigma = 0.0001, \sigma' = 0$

Figure 4: PSR and wavelet tests of stationarity on the PIF model with stochastic adaptation. Effect of $\tau_Z = 1/\lambda_Z$ on the stationarity of the ISIs. We see in (a), (b) and (c) that the smaller λ_Z is, the further the ISIs are from being stationary. τ_Z can be interpreted as a relaxation time towards a stationary regime. In (d), the absence of noise in the adaptation variable yields stationary ISIs.

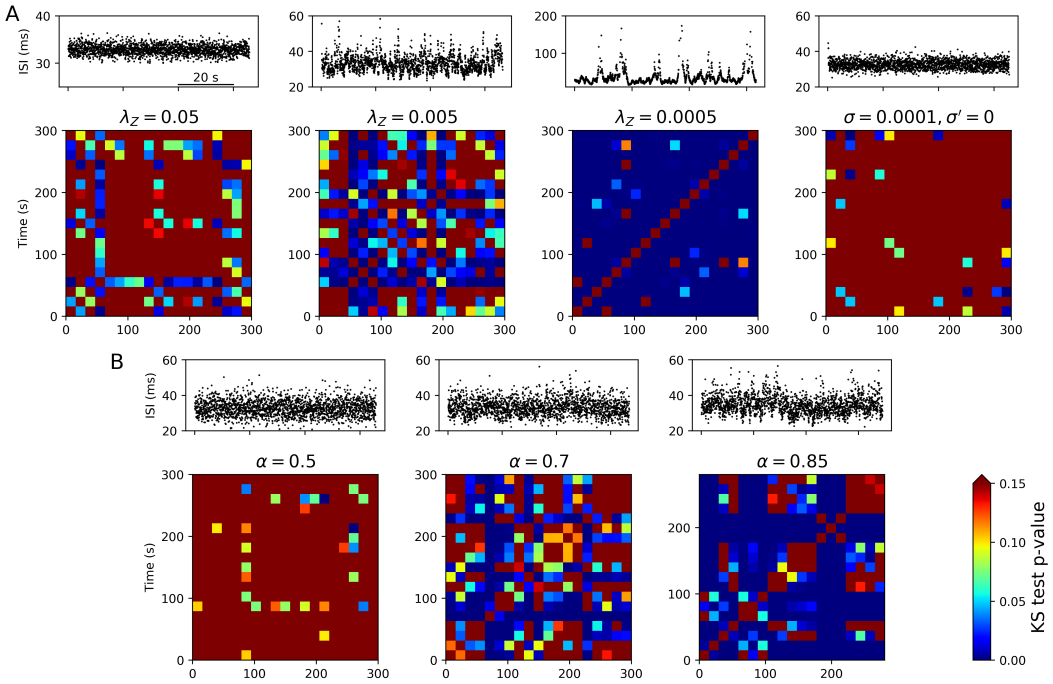

Figure 5: Windowed KS test of ISI series, for the PIF model with stochastic adaptation (**A**) and the PIF model with fractional Gaussian noise (**B**). In A, the panel for λ_Z=0.005 analyses the same data as in Figure 1, while panels for λ_Z=0.05 and λ_Z=0.0005 use the same data as in Figure 3A and B, respectively. The panel with σ=0.0001, σ'=0 corresponds to Figure 2A. In B, three values of α are shown. At the top of each panel, a sample sequence of 60 s long (around 1800 spikes) is shown. The ISI sequence analyzed in the windowed KS test is of 300 s (9000 spikes), with 20 windows of 15 s. Blue colors (p-value <0.05) indicate that the series compared are likely to be described by different distributions.

4.2 PIF model with fractional Brownian noise

We decided to compare the behavior of the Markovian PIF model with adaptation to a non-Markovian PIF model without adaptation. Therefore we set $\gamma = 0$, $\lambda_V = 0$ and explored values of α above 0.5. σ and μ were adjusted in order to obtain similar mean and variance of the ISIs obtained in the previous simulations.

4.2.1 Long-range dependence

Figure 6 shows that adding a fractional Gaussian noise indeed produces a long-term dependence in the series of ISIs, as evidenced by both Rescaled Range statistics and Detrended Fluctuation Analysis. In contrast to the PIF model with stochastic adaptation, however, the high slope in the $\log n$ versus $\log R/S(n)$ or $\log DFA(n)$ plots is maintained and does not decay as n increases. In other words, the $\hat{H}_n$ value obtained by these analyses appears to be rapidly close to its true asymptotic value. This behavior is observed at different values of α (Figure 7).
Furthermore, we see in Figure 8 that estimated Hurst parameter $\hat{H}_n$ is very close to the input value α. Hence we can safely assert that $\hat{H}_n$ converges to α.

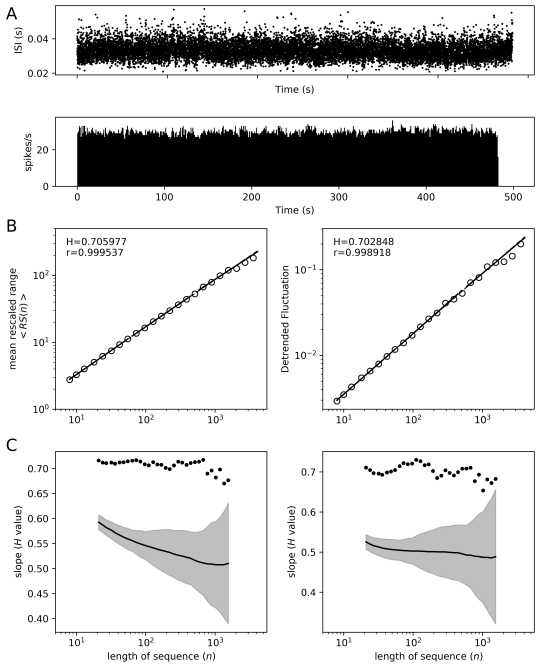

Figure 6: Long-range dependence behavior in a PIF model with fractional Gaussian noise. **A**, sequence of ISIs obtained in a simulation with equation (2) and parameters $\mu_V = 0.0303$, $\lambda_V = 0$, $\gamma = 0$, $\sigma = 0.0117$, $\alpha = 0.7$. The Z variable was not taken into account. **B**, R/S and DFA analyses for the full sequence of 14,500 spikes. The three continuous lines that depict local slopes are overlapping a segmented line that represents the best fit for all the data points. As in Figure 1C, every other point has been omitted. **C**, plot of best-fit slopes in moving windows of 15 points. The continuous line and the shadowed region are the mean and standard deviation, respectively, of the fits with surrogate data.

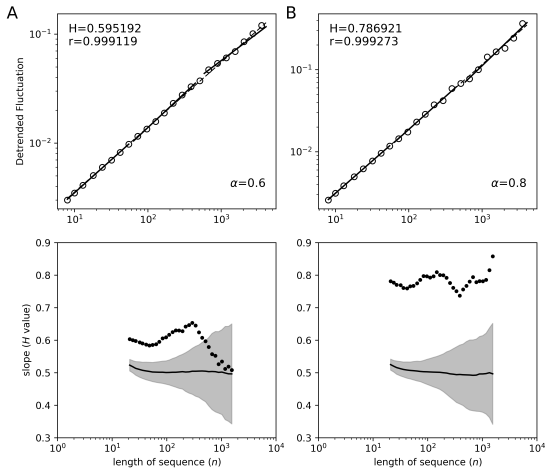

Figure 7: DF analysis of the PIF model with fractional Gaussian noise at different values of α. **A.** $\alpha = 0.6$, $\mu_V = 0.0305$, $\sigma = 0.0238$ **B.** $\alpha = 0.8$, $\mu_V = 0.0303$, $\sigma = 0.0081$. Parameters were calibrated in order to obtain similar mean and variance of the intervals as in Figure 1.

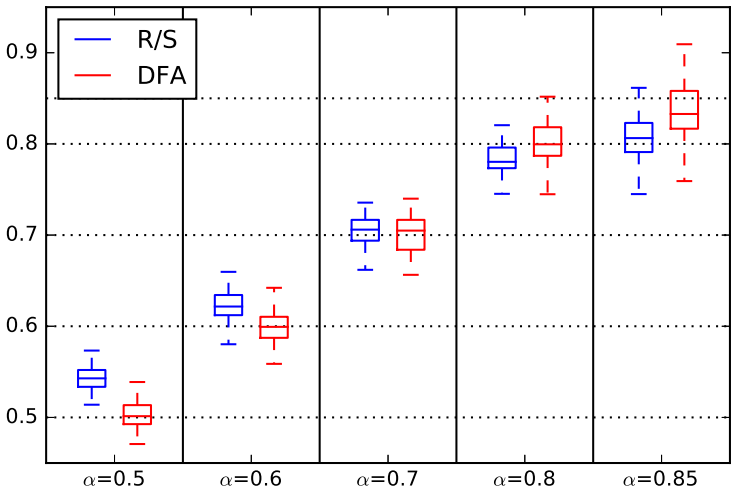

Figure 8: Measure of the Hurst parameter $\hat{H}_n$ of the fPIF model. For each $\alpha \in \{0.5, 0.6, 0.7, 0.8, 0.85\}$, we simulated 50 independent sequences of ISIs from a fPIF with parameter α (and with μ and σ chosen so that the ISIs X_n have the following moments $\mathbb{E}[X_n] \approx 32.9$ms and $\mathrm{Var}[X_n] \approx 20$). The Hurst parameter was estimated by the R/S (blue plot) and DFA (red plot) methods for each simulation, and for each underlying α parameter, the result has been aggregated in a boxplot. We see that the estimated Hurst parameter of the ISIs is very close to the value of the scaling parameter of the fBm used in the simulations. The DFA method seems to perform better.

4.2.2 Stationarity

Results concerning stationarity of this model are shown in Figure 5B for the KS test, and in Figure 9 for the PSR and wavelet tests.
We conclude unquestionably that the ISIs are stationary when $\alpha = 0.5$ (Figure 9(a)). This agrees with the theoretical result in this simple framework. The conclusion from the case $\alpha = 0.7$ - Figure 9(b)- is less straightforward, since the PSR test clearly rejects stationarity, unlike the wavelet-based test. However, we doubt that there will be a phase transition in the stationarity property for some $0.5 < \alpha_0 < 1$ (meaning that the ISIs would be stationary for $\alpha < \alpha_0$ and not stationary for $\alpha > \alpha_0$). Hence the stationarity property must be the same for any $\alpha \in (0.5, 1)$. Unlike the Markovian model, we have no mathematical reason to believe that the ISIs generated from the fractional PIF model may reach a stationary regime. Since the plots in Figure 9(c) encourage us to reject stationarity, we conclude that for any $\alpha > 0.5$, the fPIF generates non-stationary ISIs.

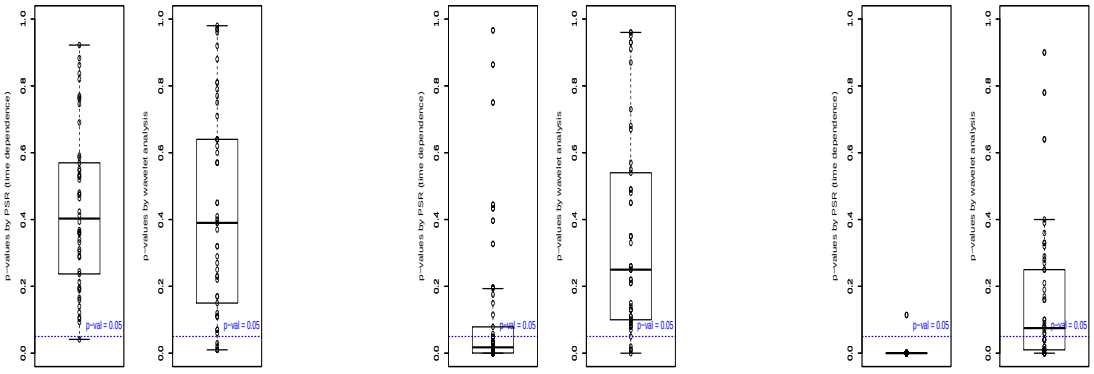

(a) $\alpha = 0.5$ (b) $\alpha = 0.7$ (c) $\alpha = 0.85$

Figure 9: PSR and wavelet tests of stationarity on the fPIF model. For each $\alpha \in \{0.5, 0.7, 0.85\}$, we use the same 50 sequences of ISIs drawn from an fPIF model (see Figure 8). In (a), the p-values of each sequence drawn from a standard PIF ($\alpha = 0.5$) are computed from the PSR test (left) and the wavelet-based test (right). The same procedure is applied to the fPIF with $\alpha = 0.7$, plot (b), and $\alpha = 0.85$, plot (c).

4.3 Other models

4.3.1 PIF model with Brownian and fractional Brownian noise

Considering Remark 3.1 and the heuristics from Section 5.2, one is tempted to consider the following modification of our model (2), where the scaling parameter of the noise in the voltage is $\frac{1}{2}$ and is $\alpha > \frac{1}{2}$ in the adaptation variable:

$$\begin{aligned} \mathrm{d}V_t &= (\mu - \lambda_V V_t + \gamma Z_t)\,\mathrm{d}t + \sigma \mathrm{d}B_t^{1/2} \\ \mathrm{d}Z_t &= (-\lambda_Z Z_t)\,\mathrm{d}t + \sigma' \mathrm{d}\tilde{B}_t^{\alpha} \end{aligned} \tag{3}$$

This model may allow for more complex behaviours, e.g. observations from simulations on the previous model display several firing regimes:

- if $\sigma = 0$ and for $\lambda_Z > 0, \lambda_V = 0, \gamma = 0.1\mu$, the estimated Hurst parameter of the ISIs, $\hat{H}_n$, remains close to the scaling parameter α of the model.
- if $\sigma > 0$ and $\sigma' \ll \sigma$, the ISIs are almost independent and $\hat{H}_n$ is close to $\frac{1}{2}$.
- if $\sigma \ll \sigma'$ and $\mu \ll 1$, then similarly to the biological data, $\hat{H}_n$ increases with n towards the value α (see Figure 10). The ISI histogram seems to deviate from the inverse Gaussian distribution (see bottom left plot in Figure 10).

Furthermore, it would be interesting to see if this model shares the multiple time scale adaptation observed by Lundstrom et al. [30] and modelled by fractional differentiation or cascade processes[3] [19].

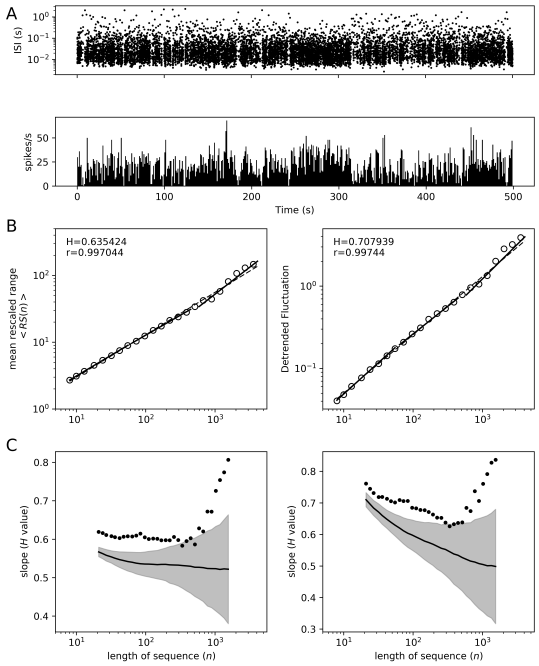

Figure 10: Simulation of 8757 spikes from the model (3) with parameters: $\mu = 0.02, \lambda_V = 0, \gamma = 0.1, \sigma = 0.007$ and $\lambda_Z = 1, \sigma' = 1, \alpha = 0.7$. The Hurst estimator $\hat{H}_n$ seems to start from lower value and increase with n.

4.3.2 Leaky Integrate-and-Fire models

The leaky Integrate-and-Fire model corresponds to $\lambda_V > 0$ in Equation (2), instead of $\lambda_V = 0$ for the PIF. We draw the same conclusions on the LRD property for the LIF (not shown). See Section 4.4 below for a summary of the properties of the PIF and LIF models.

4.3.3 Higher dimensional Integrate-and-Fire models with Brownian noise

Following the idea in [48], we simulated a PIF with three noisy adaptation variables whose time constants are $200ms$, $1000ms$ and $5000ms$ (Figure 11**A**). The aim is to get a better approximation of long-range dependence with a Markovian model. We observe in Figure 11**A** that

[3] i.e. a cascade of nested process with different relaxation times, a similar idea to nested Markov embeddings of [48].

the Hurst estimation decays more slowly in this new model, indicating that it can be a good approximation of a LRD sequence when the length is not too large. Yet it still seems to converge to $\frac{1}{2}$, which means that it is still not LRD. To emphasize the slower convergence of the LRD estimator in the multidimensional model, we compared it to the previous PIF model (from Subsection 4.1) with a large time constant of $5000ms$ (Figure 11**B**).

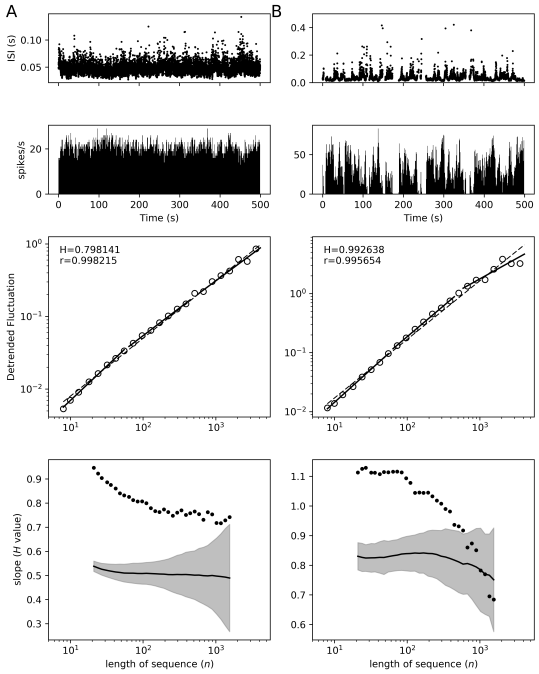

Figure 11: Long-range dependence in the PIF model with multidimensional noise. In **A**, a PIF with a single time constant ($\tau = 5000$ms) is simulated and the Hurst parameter decreases to 0.5, even with a large time constant. This is coherent with the results of Section 4.1.1. On the other hand in **B**, a PIF with three-dimensional noise whose time constants are $200ms$, $1000ms$ and $5000ms$ is simulated and we observe a slower decay of the Hurst estimation. But in both cases, the slope is negative, unlike the fractional PIF model (Fig. 6 and 7).

We observe (particularly in Figure 11 **B**) that the mean curve of the surrogate data can be higher than 0.5 for the DFA, although it decreases[4]. This is indeed a drawback of the DFA, which is not robust to data with very large mean and/or variance[5].

4.4 Summary of results on LRD and stationarity

4.4.1 Hurst estimation

The results of our numerical experiments (see Figures 7, 8 and 10) are the following:

Result 4.1. *1. Any sequence of ISIs generated by a fractional ($\alpha \in [\frac{1}{2}, 1)$) PIF/LIF with no adaptation variable ($\gamma = 0$), has a Hurst parameter equal to the scaling parameter of the underlying fBm, i.e. $\hat{H}_n \to \alpha$ as $n \to +\infty$.*

[4] we checked that it indeed decreases to 0.5 for longer spike trains.

[5] we confirmed this either by artificially removing the largest ISIs (hence reducing drastically the variance), or by simulating sequences of iid positive random variables following a Pareto law (with scale 1 and shape parameter between 1 and 2). In that situation, a strong bias appears, unlike the R/S which still returns values close to 0.5.

2. *Any sequence of ISIs generated by a Brownian ($\alpha = \frac{1}{2}$) PIF/LIF with adaptation ($\gamma \neq 0$), has a Hurst parameter equal to $\frac{1}{2}$, i.e. $\hat{H}_n \to \frac{1}{2}$ as $n \to +\infty$.*
3. *The case of PIF/LIF with a fractional stochastic adaptation variable is less straightforward, and $\hat{H}_n$ strongly depends on the parameters of the model. See the discussion below Equation (3).*

In this paragraph, let us denote by $\hat{H}_n^{\mathrm{R/S}}$ (resp. $\hat{H}_n^{\mathrm{DF}}$) the Hurst parameter computed from the R/S statistics (resp. Detrended Fluctuation Analysis). We see from Figure 8 that the DFA method gives better result than the R/S on this set of data. Indeed, the case $\alpha = 0.5$ (leftmost column) corresponds to the simplest case where the ISIs are independent and identically distributed, with finite moments. Thus we know that $\hat{H}_n^{\mathrm{R/S}}$ must converge to $\frac{1}{2}$. Hence it appears clearly that $\hat{H}_n^{\mathrm{R/S}}$ is strongly biased, unlike $\hat{H}_n^{\mathrm{DF}}$. A correction is proposed in [57] but it is only consistent with $\alpha = 0.5$.

4.4.2 Stationarity of the ISIs

The stationarity in the Markovian case was addressed in Section 5.2 from a theoretical point of view. The numerical results seem to confirm our analysis (Figures 4 and 5A): the sequence is likely to have a stationary regime, but it may be far from it, the rate of convergence to this regime being somehow related to $\tau_Z = 1/\lambda_Z$. This has practical consequences, since non-stationary time series cannot be analysed, in general, with the same methods as stationary time series.

We concluded in Section 4.2, based on observations from Figures 5B and 9, that the ISIs from the fractional PIF model with $\alpha > 0.5$ are non-stationary.

5 Discussion

In this paper, we have shown two approaches to model the *long-range* temporal correlations – sometimes called memory effect– observed in the spike trains of certain neurons (see in particular [4, 26, 29, 55] and our Introduction for more details). In a first approach, the introduction of a stochastic adaptation term into an Integrate-and-Fire model produces an apparent long-range dependence in the spikes intervals; however this property is lost when a sufficiently large sequence is analyzed. A second approach is also of the Integrate-and-Fire type, with a stochastic input called fractional Brownian motion. To the best of our knowledge, this is the first time this stochastic process is used in an IF model, and we showed that it is very well suited to produce genuine long-range dependent spike trains. Besides, this type of stationary Gaussian noise emerges naturally as a scaling limit of discrete noises (see Sections 5.1 and 5.2) which can originate either from the fractal behaviour of ion channels or from the cumulated inputs of the neuronal network.

To measure the long-range dependence of spike trains, we followed a well-established procedure (Taqqu et al. [53]), which neuroscience has already benefited from (DFA analysis of ISIs in Bhattacharya et al. [4], R/S analysis for ion channels in de Oliveira et al. [13][6]). In the literature to date, we have identified several types of IF models aimed at producing correlated spike trains: those with colored noise input, i.e. Ornstein-Uhlenbeck noise ([6, 27, 35, 46, 47]), non-renewal point processes input[7] ([2, 24, 28, 29, 54, 56]), those with $1/f$ noise input [50] and very recently PIF with high-dimensional Ornstein-Uhlenbeck noise [48]. The first conclusion of our study is that the ISIs generated from *Markovian* integrate-and-fire models –such as the one

[6] It is interesting to notice that in [13], the authors mention that the two models they proposed to replicate the observed LRD failed based on this criterion. Would an fBm-based model give better results?

[7] a limitation of the point process approach is that it is far from the biological reality.

proposed in [6, 27, 35, 46, 47, 48]– do not have long memory *stricto sensu*, and produce instead ISIs whose correlations are exponentially decaying[8]. However, as seen in all Figures 1 to 3, these Markovian integrate-and-fire models (whether perfect of leaky) can replicate a memory effect for sequences of spikes with a given length (see Figure 1), if the adaptation variable is noisy and its time constant $1/\lambda_Z$ is adequately chosen. Nonetheless, plots of the estimated Hurst parameter as a function of the sequence length are always decreasing. This contrasts with fractional integrate-and-fire models, for which this function appears constant at a value $\hat{H}$ (see Figure 6). This provides a simple criterion to discriminate between Markovian and fractional IF models. This becomes more and more obvious as the length of the spike train increases. Moreover, we see in Figures 7 and 8 that $\hat{H}$, the estimated Hurst index of the spike trains, is exactly the scaling parameter α of the fractional Brownian motion injected in the model.

We also presented and compared the effectiveness of several stationarity tests suited to time series analysis. Unlike the classical LRD treatment used here, the methodology for testing stationarity we propose seems relatively new to the neuroscience literature. Stationarity is often believed to hold for ISIs [48], yet it produced surprising results since we observed that sequences of ISIs can be non-stationary (Figures 4 and 5), even when generated from a simple LIF model with Ornstein-Uhlenbeck noise. However, we believe that a stationary regime exists for such models, and that we may have observed transitory regime with very large time constants. The case with presence of an adaptation mechanism is less clear. Meanwhile, the ISIs obtained from the fractional LIF are not stationary.
This stationarity property has important consequences: if a sequence of ISIs has a stationary regime and its correlations decay exponentially fast, then the estimated Hurst of the R/S statistic must be $\frac{1}{2}$. Altogether the present discussion on stationarity leaves several questions unanswered and should be the purpose of future work.

A very interesting and important problem that we may also be the content of future work is *calibration*. Consider the following situation: given an observed spike train with measured Hurst parameter $\hat{H} > 0.5$, we want to calibrate either the parameters μ_V, σ and α of a fractional PIF[9] or the parameters $\mu_V, \gamma, \sigma, \lambda_Z, \sigma'$ of a Markovian ($\alpha = \frac{1}{2}$) PIF with an adaptation variable. In the first case, it results from Figure 8 that we must choose $\alpha = \hat{H}$. We only have two more parameters to fix, and the mean of the ISIs is given by $\frac{1}{\mu_V}$ (assuming implicitly that the threshold is 1). We can then try to compute σ from the variance of the ISIs and $\hat{H}$. On the other hand, we have seen from Figure 3 that the $\hat{H}$ value can be replicated by adjusting λ_V: a larger λ_V yields smaller $\hat{H}$ parameter, but also impacts the first two moments of the ISIs. Hence it may be easier to fix first the scaling parameter of the noise, rather than having additional parameters just to replicate the correlations of the ISIs. Then we can focus on additional properties that adaptation can bring to integrate-and-fire models.

5.1 Other classes of models with fractal/LRD behaviour

Despite the numerous articles emphasizing the presence of fractal and/or long-range dependence of the spiking activity of some neurons (see Introduction), we merely identified two streams of papers proposing a model reflecting these characteristics.
In Jackson [24] (see references therein from related previous works from the 90's, including in particular Lowen et al. [28] and coworkers), an integrate-and-fire model is used in conjunction with various point processes modelling a random input into the neuron. If the point process is a renewal process, then it may produce long-range dependence only if it has infinite variance

[8] From this perspective, we must however point out [48] whose precise goal was to replicate power-law decay of the correlations. This is certainly achieved on a reasonable band of frequency (see the power spectrum of their simulated spike trains), but from the viewpoint of LRD, their approach falls into the limitations of any Markovian model.

[9] one could also try to calibrate (3) but this would go beyond the content of the present discussion.

([24, Theorem 2]). Infinite variance models can get far from biological observations, thus a more sophisticated point process, the fractional-Gaussian-noise-driven Poisson process (fGNDP), is used in [24]. The fGNDP is a doubly stochastic Poisson process, whose (stochastic) rate function is a nonlinear function of a fractional Gaussian noise. When injected in an IF model, this model is successful in producing spike trains with long-range dependence (as measured with the Fano factor). The idea is to consider that each jump of the fGNDP is due to a spike in a presynaptic neuron. However, the use of such process seems less mathematically tractable than our approach with a fractional noise. In fact, the fBm is itself the scaling limit of discrete processes [20, 22, 51, 52], is statistically self-similar and with stationary increments, which makes it a natural candidate as input noise.

The second approach to model LRD is an Integrate-and-Fire model with $1/f$ noise proposed by Sobie et al. [50], strongly related to our model. The link between fractional Brownian motion and $1/f$ noise is explained in Abry et al. [1]. An advantage of using fBm is that it can be exactly simulated, which ensures that all frequencies are present in its spectrum and that LRD holds, while a simulated $1/f$ noise is an approximate $1/f$ noise with limited bandwidth. Besides, a $1/f$ noise does not uniquely define a random mathematical object[10], unlike the fBm which is the only Gaussian process with given self-similarity parameter α and with stationary increments. Nevertheless, the approach of Sobie et al. [50] is complementary to ours since this study focuses on the dispersion of spike trains in time windows $[0, t]$ for various times t (as measured by the Fano factor).

5.2 Heuristics on long-range dependence and fractional Brownian motion

In classical Markovian models (e.g. PIF model with multidimensional Ornstein-Uhlenbeck noise, $\alpha = \frac{1}{2}$), the correlation between interspike i and $i+n$ decays exponentially in n, even though having high-dimensional OU process is intended to produce large time constants. We assert that the ISIs of this model are mixing, i.e. that $\sup_{A,B} |\mathbb{P}(X_i \in A, X_{i+n} \in B) - \mathbb{P}(X_i \in A)\mathbb{P}(X_{i+n} \in B)| \leq \phi(n)$, for some ϕ such that $\sum_n \phi(n) < \infty$. We also believe, based on mathematical arguments and some numerical evidence (see Section 4), that such model produces ISIs which converge to a stationary regime.

From Doukhan [18], Chapter 1.5, it is known that any stationary and mixing sequence satisfies an invariance principle. This is enough to apply Theorem 4 of Mandelbrot [31], which gives the convergence of $N^{-1/2}R/S(N)$ to a non-trivial random variable. Therefore we conjecture the following result that we plan to prove in a separate work:

Result 5.1. *If $\alpha = \frac{1}{2}$, the sequence of interspike intervals generated by the PIF/LIF model (2) has a stationary regime, and $N^{-1/2}R/S(N)$ converges to a non-degenerate random variable (i.e. $\hat{H}_N \to \frac{1}{2}$).*

Our second heuristics is about the approximation of the fractional Brownian motion by a sequence of n-dimensional Ornstein-Uhlenbeck processes, as n increases. In [48], the general idea is that the covariance of a general Gaussian process can be approximated by an Ornstein-Uhlenbeck with sufficiently many components. In [9], it is proved that the fBm is indeed an infinite-dimensional Ornstein-Uhlenbeck process. Therefore, we can consider our model with fractional noise as a natural limit to the model proposed in [48]. Although this is not the only possible limit in their approach, the fBm is the most sensible choice to obtain long-range dependence.

[10] it is not clear that there exists a stationary noise with a pure $1/f$, or $1/f^{2\alpha}$ for some $\alpha \in (0, 1)$, spectrum for all frequencies.

References

[1] P. Abry, P. Gonçalvès, and P. Flandrin. *Wavelets, spectrum analysis and 1/f processes*, pages 15–29. Springer New York, New York, NY, 1995. ISBN 978-1-4612-2544-7. doi: 10.1007/978-1-4612-2544-7_2. URL http://dx.doi.org/10.1007/978-1-4612-2544-7_2.

[2] W. Bair, C. Koch, W. Newsome, and K. Britten. Power spectrum analysis of bursting cells in area mt in the behaving monkey. *Journal of Neuroscience*, 14(5):2870–2892, 1994. ISSN 0270-6474. URL http://www.jneurosci.org/content/14/5/2870.

[3] J. Beran, Y. Feng, S. Ghosh, and R. Kulik. *Long-memory processes*. Springer, Heidelberg, 2013. ISBN 978-3-642-35511-0; 978-3-642-35512-7. doi: 10.1007/978-3-642-35512-7. URL http://dx.doi.org/10.1007/978-3-642-35512-7. Probabilistic properties and statistical methods.

[4] J. Bhattacharya, J. Edwards, A. Mamelak, and E. Schuman. Long-range temporal correlations in the spontaneous spiking of neurons in the hippocampal-amygdala complex of humans. *Neuroscience*, 131(2):547–555, 2005. ISSN 0306-4522. doi: http://doi.org/10.1016/j.neuroscience.2004.11.013. URL http://www.sciencedirect.com/science/article/pii/S0306452204010899.

[5] R. N. Bhattacharya, V. K. Gupta, and E. Waymire. The Hurst effect under trends. *J. Appl. Probab.*, 20(3):649–662, 1983. ISSN 0021-9002.

[6] N. Brunel and S. Sergi. Firing frequency of leaky intergrate-and-fire neurons with synaptic current dynamics. *Journal of Theoretical Biology*, 195(1):87–95, 1998. ISSN 0022-5193. doi: http://dx.doi.org/10.1006/jtbi.1998.0782. URL http://www.sciencedirect.com/science/article/pii/S0022519398907822.

[7] A. Cardinali and G. P. Nason. Costationarity of locally stationary time series. *J. Time Ser. Econom.*, 2(2):Art. 1, 33, 2010. ISSN 2194-6507. doi: 10.2202/1941-1928.1074. URL http://dx.doi.org/10.2202/1941-1928.1074.

[8] A. Cardinali and G. P. Nason. Practical powerful wavelet packet tests for second-order stationarity. *Applied and Computational Harmonic Analysis*, pages –, 2016. ISSN 1063-5203. doi: http://doi.org/10.1016/j.acha.2016.06.006. URL http://www.sciencedirect.com/science/article/pii/S1063520316300331.

[9] P. Carmona, L. Coutin, and G. Montseny. Approximation of some Gaussian processes. *Stat. Inference Stoch. Process.*, 3(1-2):161–171, 2000. ISSN 1387-0874. doi: 10.1023/A:1009999518898. URL http://dx.doi.org/10.1023/A:1009999518898. 19th "Rencontres Franco-Belges de Statisticiens" (Marseille, 1998).

[10] M. J. Chacron, K. Pakdaman, and A. Longtin. Interspike interval correlations, memory, adaptation, and refractoriness in a leaky integrate-and-fire model with threshold fatigue. *Neural Computation*, 15(2):253–278, 2003. doi: 10.1162/089976603762552915. URL http://dx.doi.org/10.1162/089976603762552915.

[11] A. M. Churilla, W. A. Gottschalke, L. S. Liebovitch, L. Y. Selector, A. T. Todorov, and S. Yeandle. Membrane potential fluctuations of human t-lymphocytes have fractal characteristics of fractional brownian motion. *Annals of Biomedical Engineering*, 24(1):99–108, 1995. ISSN 1573-9686. doi: 10.1007/BF02770999. URL http://dx.doi.org/10.1007/BF02770999.

[12] J.-F. Coeurjolly. Simulation and identification of the fractional brownian motion: a bibliographical and comparative study. *Journal of Statistical Software*, 5(1):1–53, 2000. ISSN 1548-7660. doi: 10.18637/jss.v005.i07. URL https://www.jstatsoft.org/index.php/jss/article/view/v005i07.

[13] R. C. de Oliveira, C. Barbosa, L. Consoni, A. Rodrigues, W. Varanda, and R. Nogueira. Long-term correlation in single calcium-activated potassium channel kinetics. *Physica A: Statistical Mechanics and its Applications*, 364:13–22, 2006. ISSN 0378-4371. doi: http://doi.org/10.1016/j.physa.2005.08.057. URL http://www.sciencedirect.com/science/article/pii/S0378437105008836.

[14] L. Decreusefond and D. Nualart. Hitting times for Gaussian processes. *Ann. Probab.*, 36(1):319–330, 2008. ISSN 0091-1798. doi: 10.1214/009117907000000132. URL http://dx.doi.org/10.1214/009117907000000132.

[15] M. Delorme and K. J. Wiese. Maximum of a fractional Brownian motion: analytic results from perturbation theory. *Phys. Rev. Lett.*, 115(21):210601, 5, 2015. ISSN 0031-9007. doi: 10.1103/PhysRevLett.115.210601. URL http://dx.doi.org/10.1103/PhysRevLett.115.210601.

[16] A. Destexhe, M. Rudolph, and D. Paré. The high-conductance state of neocortical neurons in vivo. *Nat Rev Neurosci*, 4(9):739–751, 2003. URL http://dx.doi.org/10.1038/nrn1198.

[17] T. Dieker. URL http://www.columbia.edu/~ad3217/fbm.html.

[18] P. Doukhan. *Mixing*, volume 85 of *Lecture Notes in Statistics*. Springer-Verlag, New York, 1994. ISBN 0-387-94214-9. doi: 10.1007/978-1-4612-2642-0. URL http://dx.doi.org/10.1007/978-1-4612-2642-0. Properties and examples.

[19] P. J. Drew and L. F. Abbott. Models and properties of power-law adaptation in neural systems. *Journal of Neurophysiology*, 96(2):826–833, 2006. ISSN 0022-3077. doi: 10.1152/jn.00134.2006. URL http://jn.physiology.org/content/96/2/826.

[20] N. Enriquez. A simple construction of the fractional Brownian motion. *Stochastic Process. Appl.*, 109(2):203–223, 2004. ISSN 0304-4149. doi: 10.1016/j.spa.2003.10.008. URL http://dx.doi.org/10.1016/j.spa.2003.10.008.

[21] G. L. Gerstein and B. Mandelbrot. Random walk models for the spike activity of a single neuron. *Biophysical Journal*, 4(1):41 – 68, 1964. ISSN 0006-3495. doi: http://dx.doi.org/10.1016/S0006-3495(64)86768-0. URL http://www.sciencedirect.com/science/article/pii/S0006349564867680.

[22] A. Hammond and S. Sheffield. Power law Pólya's urn and fractional Brownian motion. *Probab. Theory Related Fields*, 157(3-4):691–719, 2013. ISSN 0178-8051. doi: 10.1007/s00440-012-0468-6. URL http://dx.doi.org/10.1007/s00440-012-0468-6.

[23] A. L. Hodgkin and A. F. Huxley. A quantitative description of membrane current and its application to conduction and excitation in nerve. *The Journal of Physiology*, 117(4):500–544, 1952. URL http://www.ncbi.nlm.nih.gov/pmc/articles/PMC1392413/.

[24] B. S. Jackson. Including long-range dependence in integrate-and-fire models of the high interspike-interval variability of cortical neurons. *Neural Computation*, 16(10):2125–2195, 2004. doi: 10.1162/0899766041732413. URL http://dx.doi.org/10.1162/0899766041732413.

[25] D. Kwiatkowski, P. C. Phillips, P. Schmidt, and Y. Shin. Testing the null hypothesis of stationarity against the alternative of a unit root. *Journal of Econometrics*, 54(1):159 – 178, 1992. ISSN 0304-4076. doi: http://dx.doi.org/10.1016/0304-4076(92)90104-Y. URL http://www.sciencedirect.com/science/article/pii/030440769290104Y.

[26] C. D. Lewis, G. L. Gebber, P. D. Larsen, and S. M. Barman. Long-term correlations in the spike trains of medullary sympathetic neurons. *Journal of Neurophysiology*, 85(4):1614–1622, 2001. ISSN 0022-3077. URL http://jn.physiology.org/content/85/4/1614.

[27] B. Lindner. Interspike interval statistics of neurons driven by colored noise. *Phys. Rev. E*, 69:022901, Feb 2004. doi: 10.1103/PhysRevE.69.022901. URL https://link.aps.org/doi/10.1103/PhysRevE.69.022901.

[28] S. B. Lowen, S. S. Cash, M.-m. Poo, and M. C. Teich. Quantal neurotransmitter secretion rate exhibits fractal behavior. *Journal of Neuroscience*, 17(15):5666–5677, 1997. ISSN 0270-6474. URL http://www.jneurosci.org/content/17/15/5666.

[29] S. B. Lowen, T. Ozaki, E. Kaplan, B. E. Saleh, and M. C. Teich. Fractal features of dark, maintained, and driven neural discharges in the cat visual system. *Methods*, 24(4): 377 – 394, 2001. ISSN 1046-2023. doi: http://dx.doi.org/10.1006/meth.2001.1207. URL http://www.sciencedirect.com/science/article/pii/S1046202301912071.

[30] B. N. Lundstrom, M. H. Higgs, W. J. Spain, and A. L. Fairhall. Fractional differentiation by neocortical pyramidal neurons. *Nat Neurosci*, 11(11):1335–1342, 11 2008.

[31] B. B. Mandelbrot. Limit theorems on the self-normalized range for weakly and strongly dependent processes. *Z. Wahrscheinlichkeitstheorie und Verw. Gebiete*, 31:271–285, 1974/75. doi: 10.1007/BF00532867. URL http://dx.doi.org/10.1007/BF00532867.

[32] B. B. Mandelbrot and J. R. Wallis. Noah, joseph, and operational hydrology. *Water Resources Research*, 4(5):909–918, 1968. ISSN 1944-7973. doi: 10.1029/WR004i005p00909. URL http://dx.doi.org/10.1029/WR004i005p00909.

[33] B. B. Mandelbrot. Une classe de processus stochastiques homothétiques à soi; application à la loi climatologique H. E. Hurst. *C. R. Acad. Sci. Paris*, 260:3274–3277, 1965.

[34] R. Metzler and J. Klafter. The restaurant at the end of the random walk: recent developments in the description of anomalous transport by fractional dynamics. *J. Phys. A*, 37(31):R161–R208, 2004. ISSN 0305-4470. doi: 10.1088/0305-4470/37/31/R01. URL http://dx.doi.org/10.1088/0305-4470/37/31/R01.

[35] J. W. Middleton, M. J. Chacron, B. Lindner, and A. Longtin. Firing statistics of a neuron model driven by long-range correlated noise. *Phys. Rev. E*, 68:021920, Aug 2003. doi: 10.1103/PhysRevE.68.021920. URL https://link.aps.org/doi/10.1103/PhysRevE.68.021920.

[36] G. Nason. A test for second-order stationarity and approximate confidence intervals for localized autocovariances for locally stationary time series. *J. R. Stat. Soc. Ser. B. Stat. Methodol.*, 75(5):879–904, 2013. ISSN 1369-7412. doi: 10.1111/rssb.12015. URL http://dx.doi.org/10.1111/rssb.12015.

[37] C.-K. Peng, S. V. Buldyrev, A. L. Goldberger, S. Havlin, F. Sciortino, M. Simon, and H. E. Stanley. Long-range correlations in nucleotide sequences. *Nature*, 356:168–170, 1992.

[38] C.-K. Peng, J. Mietus, J. M. Hausdorff, S. Havlin, H. E. Stanley, and A. L. Goldberger. Long-range anticorrelations and non-gaussian behavior of the heartbeat. *Phys. Rev. Lett.*, 70:1343–1346, Mar 1993. doi: 10.1103/PhysRevLett.70.1343. URL https://link.aps.org/doi/10.1103/PhysRevLett.70.1343.

[39] C.-K. Peng, S. V. Buldyrev, S. Havlin, M. Simons, H. E. Stanley, and A. L. Goldberger. Mosaic organization of dna nucleotides. *Phys. Rev. E*, 49:1685–1689, Feb 1994. doi: 10.1103/PhysRevE.49.1685. URL https://link.aps.org/doi/10.1103/PhysRevE.49.1685.

[40] M. B. Priestley and T. Subba Rao. A test for non-stationarity of time-series. *J. Roy. Statist. Soc. Ser. B*, 31:140–149, 1969. ISSN 0035-9246. URL http://links.jstor.org/sici?sici=0035-9246(1969)31:1<140:ATFNOT>2.0.CO;2-V&origin=MSN.

[41] G. Rangarajan and M. Ding, editors. *Processes with long-range correlations: Theory and applications*, volume 621 of *Lecture Notes in Physics*. Springer-Verlag Berlin Heidelberg, 2003.

[42] D. Revuz and M. Yor. *Continuous martingales and Brownian motion*, volume 293 of *Grundlehren der Mathematischen Wissenschaften [Fundamental Principles of Mathematical Sciences]*. Springer-Verlag, Berlin, third edition, 1999. ISBN 3-540-64325-7. doi: 10.1007/978-3-662-06400-9. URL http://dx.doi.org/10.1007/978-3-662-06400-9.

[43] A. Richard and D. Talay. Hölder continuity in the Hurst parameter of functionals of Stochastic Differential Equations driven by fractional Brownian motion. *arXiv preprint arXiv:1605.03475*, 2016.

[44] L. Sacerdote and M. T. Giraudo. Stochastic integrate and fire models: a review on mathematical methods and their applications. In *Stochastic biomathematical models*, volume 2058 of *Lecture Notes in Math.*, pages 99–148. Springer, Heidelberg, 2013. doi: 10.1007/978-3-642-32157-3_5. URL http://dx.doi.org/10.1007/978-3-642-32157-3_5.

[45] G. Samorodnitsky. *Stochastic processes and long range dependence*. Springer Series in Operations Research and Financial Engineering. Springer, Cham, 2016. ISBN 978-3-319-45574-7; 978-3-319-45575-4. doi: 10.1007/978-3-319-45575-4. URL http://dx.doi.org/10.1007/978-3-319-45575-4.

[46] T. Schwalger and L. Schimansky-Geier. Interspike interval statistics of a leaky integrate-and-fire neuron driven by gaussian noise with large correlation times. *Phys. Rev. E*, 77:031914, Mar 2008. doi: 10.1103/PhysRevE.77.031914. URL https://link.aps.org/doi/10.1103/PhysRevE.77.031914.

[47] T. Schwalger, K. Fisch, J. Benda, and B. Lindner. How noisy adaptation of neurons shapes interspike interval histograms and correlations. *PLoS Comput. Biol.*, 6(12):e1001026, 25, 2010. ISSN 1553-734X. doi: 10.1371/journal.pcbi.1001026. URL http://dx.doi.org/10.1371/journal.pcbi.1001026.

[48] T. Schwalger, F. Droste, and B. Lindner. Statistical structure of neural spiking under non-Poissonian or other non-white stimulation. *J. Comput. Neurosci.*, 39(1):29–51, 2015. ISSN 0929-5313. doi: 10.1007/s10827-015-0560-x. URL http://dx.doi.org/10.1007/s10827-015-0560-x.

[49] R. Segev, M. Benveniste, E. Hulata, N. Cohen, A. Palevski, E. Kapon, Y. Shapira, and E. Ben-Jacob. Long term behavior of lithographically prepared in vitro neuronal networks. *Phys. Rev. Lett.*, 88:118102, Mar 2002. doi: 10.1103/PhysRevLett.88.118102. URL https://link.aps.org/doi/10.1103/PhysRevLett.88.118102.

[50] C. Sobie, A. Babul, and R. de Sousa. Neuron dynamics in the presence of $1/f$ noise. *Phys. Rev. E*, 83:051912, May 2011. doi: 10.1103/PhysRevE.83.051912. URL https://link.aps.org/doi/10.1103/PhysRevE.83.051912.

[51] T. Sottinen. Fractional Brownian motion, random walks and binary market models. *Finance Stoch.*, 5(3):343–355, 2001. ISSN 0949-2984. doi: 10.1007/PL00013536. URL http://dx.doi.org/10.1007/PL00013536.

[52] M. S. Taqqu. Weak convergence to fractional Brownian motion and to the Rosenblatt process. *Z. Wahrscheinlichkeitstheorie und Verw. Gebiete*, 31:287–302, 1974/75. doi: 10.1007/BF00532868. URL http://dx.doi.org/10.1007/BF00532868.

[53] M. S. Taqqu, V. Teverovsky, and W. Willinger. Estimators for long-range dependence: an empirical study. *Fractals*, 03(04):785–798, 1995. doi: 10.1142/S0218348X95000692. URL http://www.worldscientific.com/doi/abs/10.1142/S0218348X95000692.

[54] M. C. Teich. Fractal neuronal firing patterns. In T. MCKenna, J. Davis, and S. F. Zornetzer, editors, *Single Neuron Computation*, Neural Networks: Foundations to Applications, pages 589 – 625. Academic Press, San Diego, 1992. ISBN 978-0-12-484815-3. doi: http://doi.org/10.1016/B978-0-12-484815-3.50031-1. URL http://www.sciencedirect.com/science/article/pii/B9780124848153500311.

[55] M. C. Teich, R. G. Turcott, and R. M. Siegel. Temporal correlation in cat striate-cortex neural spike trains. *IEEE Engineering in Medicine and Biology Magazine*, 15(5):79–87, 1996. ISSN 0739-5175. doi: 10.1109/51.537063.

[56] M. C. Teich, C. Heneghan, S. B. Lowen, T. Ozaki, and E. Kaplan. Fractal character of the neural spike train in the visual system of the cat. *J. Opt. Soc. Am. A*, 14(3):529–546, Mar 1997. doi: 10.1364/JOSAA.14.000529. URL http://josaa.osa.org/abstract.cfm?URI=josaa-14-3-529.

[57] R. Weron. Estimating long-range dependence: finite sample properties and confidence intervals. *Phys. A*, 312(1-2):285–299, 2002. ISSN 0378-4371. doi: 10.1016/S0378-4371(02)00961-5. URL http://dx.doi.org/10.1016/S0378-4371(02)00961-5.

[58] W. Willinger, M. S. Taqqu, R. Sherman, and D. V. Wilson. Self-similarity through high-variability: Statistical analysis of ethernet lan traffic at the source level. *IEEE/ACM Trans. Netw.*, 5(1):71–86, Feb. 1997. ISSN 1063-6692. doi: 10.1109/90.554723. URL http://dx.doi.org/10.1109/90.554723.